Biomechan Model Mechanobiol (2006) 5: 217–225
DOI 10.1007/s10237-006-0018-1

ORIGINAL PAPER

**Ryan W. Kobs · Naomi C. Chesler**

# The mechanobiology of pulmonary vascular remodeling in the congenital absence of eNOS

Recevied: 11 February 2005 / Accepted: 15 December 2005 / Published online: 7 March 2006


**Abstract** Primary pulmonary hypertension is a rare but deadly disease. Lungs extracted from PPH patients are deficient in endothelial nitric oxide synthase (eNOS), making the eNOS-null mouse a potentially useful model of the disease. To better understand the progression of pulmonary vascular remodeling in the congenital absence of eNOS, we induced pulmonary hypertension in eNOS-null mice using hypobaric hypoxia, and then quantified large artery structure and function in contralateral vessels. In particular, to assess structure we quantified diameter, wall thickness, and collagen, elastin and smooth muscle cell content; to quantify function we performed pressure-diameter tests. After remodeling, the pulmonary arteries had increased wall, collagen and elastin thicknesses compared to controls ($P < 0.05$). The remodeled pulmonary arteries also had increased elastic moduli at low and high strains compared to controls ($P < 0.05$). The increases in moduli at low and high strain correlated with increases in elastin and collagen thickness, respectively ($P < 0.05$). These results provide insight into the mechanobiology of pulmonary vascular remodeling in the congenital absence of eNOS, and the coupled nature of these changes.

## 1 Introduction

Primary pulmonary hypertension (PPH) is a rare but deadly disease, principally claiming the lives of young and middle-aged women, often in 2–3 years from onset of symptoms (Rubin 1997). Recently, mutations associated with bone morphogenetic peptides have been identified in approximately 25% of cases of familial pulmonary arterial hypertension and 25% of cases of sporadic pulmonary hypertension (Lane et al. 2000; Thomson et al. 2000). For the majority of familial and sporadic cases, however, no genetic abnormalities have been identified. Since lungs extracted from PPH patients are deficient in endothelial nitric oxide synthase (eNOS) (Giaid and Saleh 1995), mice genetically-engineered to be deficient in eNOS (eNOS-null mice) are a potentially useful model for studying the disease and its progression. eNOS is one of three enzymes that produce nitric oxide (NO), which is a constitutively produced, potent vasodilator (Persson et al. 1990; Leeman et al. 1994; Blitzer 1996). Not coincidentally, inhaled nitric oxide is one treatment for persistent pulmonary hypertension of the newborn that has had some success in human trials (Abman 1999; Clark et al. 2000).

Perhaps like PPH patients in the early stages of the disease, eNOS-null mice have mild pulmonary hypertension (Fagan et al. 1999). To investigate the progression of the disease, these mice have been exposed to severe hypoxia (such that partial pressure of oxygen is reduced by 50%), which increased pulmonary vascular resistance (Steudel et al. 1997), pulmonary artery pressures, and the number of muscularized arterioles (Fagan et al. 1999). However, the remodeling of large arteries, which can affect the pulse wave energy transmission in the cardiopulmonary system and thus ventricular function (O'Rourke 1982), was not investigated. The effects of severe hypoxia, which causes severe pulmonary hypertension, on the mechanical and biological properties of large, conduit arteries in this animal model of PPH remain unknown.

The goal of this study was to quantify the mechanical and biological aspects of hypertension-induced pulmonary vascular remodeling of large pulmonary arteries in this animal model. More precisely, we investigated the effects of hypoxia-induced pulmonary hypertension on the collagen and elastin content, and elasticity and damping coefficient of large pulmonary arteries of eNOS-null mice and the correlations between these measured biological and mechanical changes.

We hypothesized that in response to severe hypoxia, collagen and elastin would accumulate in the large pulmonary arteries, and that the tissue elastic modulus would increase at

R.W. Kobs · N.C. Chesler (✉)
Department of Biomedical Engineering,
University of Wisconsin – Madison,
2146 Engineering Centers Building 1550 Engineering Drive,
Madison, WI 53706-1609, USA
E-mail: chesler@engr.wisc.edu
Tel.: +1-608-2658920
Fax: +1-608-2659239

low strain due to the increased elastin content and increase at high strain due to the increased collagen content. We tested these hypotheses with quantitative histology on right main pulmonary arteries of eNOS-null mice exposed to 0 (control), 10 and 15 days of severe hypobaric hypoxia, and isolated vessel experiments on left main pulmonary arteries. Once the sequence of mechanical and biological events in the progression of pulmonary vascular remodeling in pulmonary hypertension are better understood, novel treatment options to stop or reverse these coupled changes can be designed.

## 2 Methods

### 2.1 Animal handling

Twenty-seven male and female eNOS-null mice (B6.129P2-Nos3$^{tm1Unc}$/J, Jackson Laboratory, Bar Harbor, ME, USA) were divided into three equal groups: 0-day control, 10-day hypoxic, and 15-day hypoxic (five males and four females each group). All mice were between 6 and 8 weeks of age at the end of the 0-, 10- or 15-day experimental protocol. The mice in the 10- and 15-day hypoxic groups were exposed to hypobaric hypoxia in a small altitude (SALT) chamber at the University of Wisconsin Biotron facility. By reducing the barometric pressure from that at sea level (760 mmHg) to that at approximately 17,000 ft elevation (380 mmHg), the partial pressure of $O_2$ was reduced from approximately 160 mmHg ($= 21\% \times 760$ mmHg) to 80 mmHg ($= 21\% \times 380$ mmHg). Barometric pressure returned to sea level conditions for no more than 30 min once per day for regular animal care and maintenance. Mice were weighed at the end of the exposure period (see Table 2) and euthanized by intraperitoneal injection of 150 mg/kg pentobarbital solution. All protocols and procedures were approved by the University of Wisconsin Institutional Animal Care and Use Committee.

Left and right pulmonary arteries (PAs) were excised between the first and second pulmonary artery bifurcations and placed in fresh Dulbecco's phosphate buffered saline solution (PBS, without calcium chloride or magnesium chloride, Sigma Chemical Co., St. Louis, MO, USA). The right PA was preserved for histology in frozen sections without pressurization or fixing as done previously (Kobs et al. 2005). The left PA was mounted in an arteriograph system for mechanical testing.

### 2.2 Histology and quantitative image analysis

Histological staining and measurement of wall thickness, collagen, elastin and smooth muscle cell (SMC) content in isolated right main pulmonary arteries were performed as previously described (Kobs et al. 2005). Briefly, each vessel was slow frozen in tissue freezing medium surrounded by 2-methyl butane cooled by liquid nitrogen without pressurization or chemical fixation. At least two 5 $\mu$m sections were cut at $-20$°C on a cryostat from the proximal and distal ends of each vessel for each assay. These sections were stained with Verhoff Van Geisen (VVG) solution to identify elastin, picro-sirius red (SR) to identify collagen, and hematoxylin to measure intimal-to-adventitial wall thickness. For the VVG and SR stains, two representative fields of view (FOV) were chosen for each location (proximal or distal) by a single observer blinded to the experimental condition. The area positive for protein was identified by color thresholding in the FOV and compared to the total tissue area to produce a percent protein in the artery wall. The percent of SMC in the wall was indirectly quantified as the difference between total tissue and percent elastin plus percent collagen. That is, $\%\text{SMC} = 100\% - (\%\text{elastin} + \%\text{collagen})$. Wall thickness was measured with line measurement tools by averaging ten equally spaced positions around the whole vessel circumference for each location (proximal or distal). These measurements were also taken by a single individual blinded to the experimental condition.

For the collagen, elastin and SMC percentages and wall thickness measurements, no significant differences were found between the proximal and distal locations. Therefore, proximal and distal data for each vessel were pooled to generate a length-wise average for each measurement. Collagen, elastin or SMC thickness or content were computed as the percent collagen, elastin or SMC respectively, multiplied by the wall thickness for each vessel.

### 2.3 Mechanical testing

Left main pulmonary arteries were mounted in an arteriograph chamber in which vessels can be stretched to in vivo length, pressurized, and visualized by transillumination microscopy (Chesler et al. 2004). PBS was used to fill the arteriograph bath, buffered to maintain a constant pH of 7.4 and heated to 37°C. Calcium free PBS was used to prevent SMC contraction during testing. Pressure transducers were situated immediately up- and downstream of the vessel. An upstream in-line pressure servomechanism continually adjusted the computed average transmural pressure via computer control (LabVIEW, National Instruments, Austin, TX, USA).

Immediately after mounting, the left PA was pressurized to 5 mmHg and its unstretched length was measured suture-to-suture. The vessel was then stretched 140% to approximate in vivo axial length as measured by microcomputed tomography in representative animals exposed to 0-, 10- and 15-days of hypoxia ($n = 3$ at each timepoint, data not shown). The vessel was allowed to equilibrate in PBS at 37°C for 60 min, after which it was mechanically preconditioned by cycling the pressure five times from 5 to 60 mmHg at 0.014 Hz. The response was repeatable after the third cycle in general. The fifth cycle of data was used to measure mechanical properties under dynamic loading conditions: dynamic circumferential moduli at low and high strain and the pulse damping coefficient. To measure mechanical properties under static loading conditions, the vessel was subjected to seven pressure steps; these were from 5 to 10, 20, 30, 40, 50, 60, and again to

10 mmHg for 45 s each. Steps were separated by ten times the step duration (450 s) of rest at 5 mmHg to allow tissue recovery from previous steps (Lakes 1998). Inner diameter and left and right wall thicknesses were continuously optically measured by a video dimension analyzer (Living Systems Instrumentation, Burlington, VT, USA); these data as well as upstream and downstream pressures were sampled at 1 Hz and saved on a PC for further analysis.

### 2.4 Calculations

For the purposes of the mechanical analysis, the artery wall is assumed to be incompressible and homogeneous. Using the thin wall assumption, which is valid for radius to wall thickness (WT) ratio greater than 10, circumferential wall stress ($\sigma$) was calculated according to:

$$\sigma = \frac{\mathrm{ID}}{2\mathrm{WT}} P,$$

where $P$ is the transmural pressure, ID is the inner diameter and WT is based on the optically (not histologically) measured value. Circumferential strain ($e$) was calculated using Green's formulation for large deformations (Fung 1993) based on circumferential stretch ($\lambda$), which is the ratio of pressure-dependent, deformed circumference ($\pi$ OD) to circumference at the baseline pressure of 5 mmHg ($\pi \mathrm{OD}_5$):

$$e = \frac{1}{2}\left(\lambda^2 - 1\right), \text{ where } \lambda = \frac{\pi \mathrm{OD}}{\pi \mathrm{OD}_5} = \frac{\mathrm{OD}}{\mathrm{OD}_5}$$

Unlike thick-walled arteries, pulmonary arteries are prone to collapse at zero transmural pressure; thus, a non-zero baseline pressure is typically used (Faury et al. 1999). Collapse is to be avoided since it is likely to damage endothelial cells. Thus, the vessel state at 5 mmHg was used as an approximation of the unloaded state, which was used as the reference state in all calculations.

The static stretch response of the vessel was analyzed isochronally, 15 s into the pressure step. Two dynamic circumferential elastic moduli were calculated from the average inflation/deflation slope of the stress-strain curve: the low strain tangent ($E_{\text{low strain}}$) and the high strain tangent ($E_{\text{high strain}}$) (see Fig. 1). The damping coefficient was also calculated from the dynamic-loading stress-strain relationship. First, the strain ($e_{\tan}$) at the point in the stress–strain curve where the rate of change of the slope was a maximum was identified. Then, the stress difference between inflation and deflation at this point ($\Delta\sigma_{\tan}$) was calculated. The stress difference between the maximum and minimum stress values ($\Delta\sigma_{\max}$) was also calculated for each curve. Finally, the damping coefficient d (see Fig. 1) was computed as $\Delta\sigma_{\tan}/\Delta\sigma_{\max}$ as in (Kobs et al. 2005). For all calculations, the pressure-dependent wall thickness values WT were derived from conservation of mass assuming no axial extension and the optically measured wall thickness value at 60 mmHg (Faury et al. 1999).

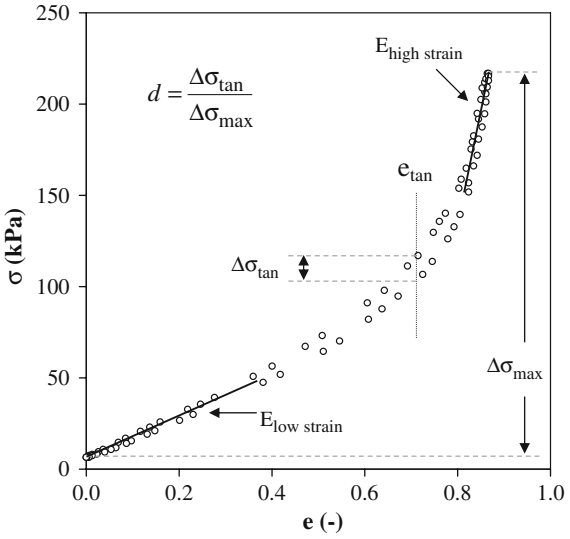


**Fig. 1** Representative PA dynamic stress-strain curve (15-day) showing elastic moduli ($E_{\text{low strain}}$ and $E_{\text{high strain}}$) and damping coefficient ($d$). See text for details

### 2.5 Statistics

ANOVA models were used to examine differences in collagen, elastin, SMC and wall thicknesses and vessel dynamic behavior between the experimental groups (0-, 10- and 15-day). Repeated measures ANOVA models were used to examine differences in collagen, elastin and SMC percent and vessel static behavior between the experimental groups. All results are presented as mean ± standard deviation.

Analyses of correlation between the mechanical and biological endpoints were performed using non-parametric Spearman's rank correlation coefficient. The regression analysis coefficient of determination ($R^2$) is reported to reflect the linearity of the correlative relationships; Spearman's correlation coefficient ($r_s$) and its associated $P$ value (if significant) is reported to reflect the trends in the data. For each significant test, a general two-sided significance level of 5% was applied. All statistical analyses were performed using SAS software (SAS Institute Inc., Cary, NC, USA) version 8.1.

## 3 Results

### 3.1 Histology and quantitative image analysis

Representative images of control and 10-day hypoxic vessels stained for VVG and SR are shown in Fig. 2. Average percentages of collagen, elastin and SMC in the artery wall of the 0-, 10- and 15-day groups are given in Table 1. While the percent elastin in the arterial wall did not significantly change with hypoxia, the percent collagen did ($P < 0.05$ for both 10-day versus control and 15-day versus control). Percent SMC at 10 days was significantly lower than at 0 days ($P < 0.05$).

Collagen, elastin, and SMC thicknesses (percent protein content multiplied by wall thickness for a given vessel) also

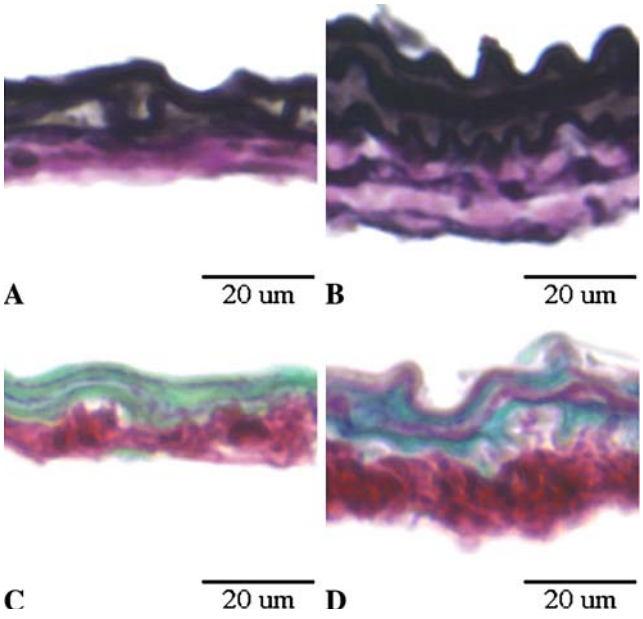


**Fig. 2** Representative images of elastin and collagen staining in PAs of eNOS-null mice. **a, b** VVG staining for elastin, which appears *black*; **c, d** SR staining for collagen, which appears *red*. **a, c** 0-day control; **b, d** 10-day hypoxia vessels. *Scale bar* is 20 $\mu$m for all images

**Table 1** Quantitative histology results for right pulmonary arteries of eNOS-null mice exposed to 0-, 10- and 15-days of hypobaric hypoxia

| | 0-day | 10-day | 15-day |
|---|---|---|---|
| Percent elastin | 31 ± 2% | 31 ± 3 % | 29 ± 3 % |
| Percent collagen | 48 ± 6% | 56 ± 5%* | 55 ± 2%* |
| Percent SMC | 20 ± 6% | 13 ± 5%* | 16 ± 4% |
| Elastin thickness ($\mu$m) | 5.6 ± 0.7 | 9.4 ± 1.5** | 9.4 ± 0.9** |
| Collagen thickness ($\mu$m) | 8.7 ± 1.6 | 17.3 ± 2.4** | 17.8 ± 1.6** |
| SMC thickness ($\mu$m) | 3.7 ± 1.4 | 3.9 ± 1.4 | 5.0 ± 1.5 |
| Wall thickness ($\mu$m) | 18 ± 3 | 31 ± 3** | 32 ± 2** |

* $P < 0.05$ versus 0-day
** $P < 0.001$ versus 0-day

were analyzed for changes with hypoxia. Elastin and collagen thicknesses increased after 10 and 15 days ($P < 0.001$ versus control for both, Table 1) whereas SMC thickness did not. Neither elastin nor collagen thickness increased between 10 and 15 days.

## 3.2 Mechanical testing

### *3.2.1 Thin wall assumption*

The thin wall assumption was found to be valid under most conditions and pressures, with exceptions at 5 mmHg for 10- and 15-day hypoxic vessels. In particular, at 5 mmHg, the ratios of inner radius to wall thickness for 0-, 10-, and 15-day vessels were 12.6 ± 1.8, 7.8 ± 1.3, and 7.5 ± 0.7, respectively. As the pressure increased, this ratio increased, validating this assumption above 10 mmHg for both hypoxic groups. At 60 mmHg the ratios for 0-, 10-, and 15-day vessels were 43.1 ± 3.1, 25.5 ± 3.3, and 24.3 ± 2.8, respectively (see Table 2 for average ID and OD).

**Table 2** Mouse body weights, PA axial lengths and optically-measured PA OD and ID ($\mu$m) for the 0-, 10-and 15-day groups taken 15 s after each static pressure step and at the initial 5 mmHg resting pressure

| | 0-day | 10-day | 15-day |
|---|---|---|---|
| Body weight (g) | | | |
| Female | 16 ± 0.4 | 14 ± 0.8* | 15 ± 0.3 |
| Male | 21 ± 2.0 | 18 ± 2.1 | 20 ± 1.5 |
| Axial Length (mm) | 2.3 ± 0.2 | 2.8 ± 0.3** | 3.0 ± 0.2** |
| 5 mmHg | | | |
| OD | 491 ± 21 | 527 ± 38* | 534 ± 33* |
| ID | 445 ± 21 | 473 ± 41 | 477 ± 34 |
| 10 mmHg | | | |
| OD | 547 ± 24 | 572 ± 40 | 577 ± 35 |
| ID | 506 ± 23 | 525 ± 41 | 528 ± 37 |
| 20 mmHg | | | |
| OD | 778 ± 58 | 687 ± 48** | 679 ± 38** |
| ID | 740 ± 61 | 646 ± 51** | 637 ± 38** |
| 30 mmHg | | | |
| OD | 1033 ± 64 | 814 ± 55** | 802 ± 46** |
| ID | 1001 ± 66 | 774 ± 56** | 763 ± 47** |
| 40 mmHg | | | |
| OD | 1113 ± 58 | 875 ± 74** | 879 ± 59** |
| ID | 1085 ± 59 | 837 ± 73** | 844 ± 60** |
| 50 mmHg | | | |
| OD | 1141 ± 60 | 892 ± 76** | 901 ± 65** |
| ID | 1115 ± 60 | 857 ± 76** | 864 ± 65** |
| 60 mmHg | | | |
| OD | 1159 ± 63 | 903 ± 76** | 912 ± 67** |
| ID | 1131 ± 62 | 869 ± 77** | 877 ± 67** |
| 10 mmHg | | | |
| OD | 546 ± 25 | 587 ± 37** | 595 ± 36** |
| ID | 504 ± 27 | 539 ± 37** | 548 ± 37** |

The final step to 10 mmHg (last two rows) was performed to verify the absence of plastic deformation due to the mechanical testing protocol.
* $P < 0.05$ versus 0-day
** $P < 0.001$ versus 0-day

### *3.2.2 Static behavior*

Optically-measured main pulmonary artery OD increased significantly with hypoxia and imposed transmural pressure (Table 2). At the baseline pressure of 5 mmHg, the 10- and 15-day hypoxic vessels were 7 and 9% larger in OD than the 0-day vessels, respectively. At the highest transmural pressure of 60 mmHg, the 10- and 15-day hypoxic vessels were 22 and 21% smaller than the 0-day vessels, respectively. The OD measured during a final step to 10 mmHg (the penultimate row in Table 2) were 2% different on average from the OD measured during the first step to 10 mmHg, indicating the absence of plastic deformation during static loading.

The static stretch response of the vessels to steps in pressure measured isochronally was greater in control vessels than hypoxic vessels at all pressures tested (Fig. 3). That is, control vessels always stretched more circumferentially in response to transmural pressure increases than hypoxic vessels. Differences were increasingly significant as the pressure steps increased in magnitude, with the greatest difference at 60 mmHg ($P < 0.001$). There was no significant

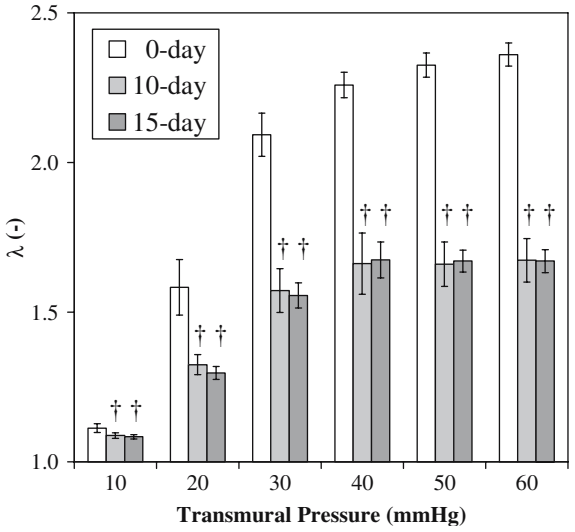


**Fig. 3** Circumferential isochronal stretch ratio for each pressure step (15 s after step) for the 0-, 10- and 15-day groups. † $P < 0.001$ versus 0-day

difference or trend between the stretch responses of the two hypoxic groups. Hypoxic groups also showed maximum stretch at 40 mmHg whereas control vessels continued to increase stretch with increasing pressure up to 60 mmHg.

### *3.2.3 Dynamic behavior*

Dynamic circumferential elastic moduli for the 0-, 10- and 15-day vessels were determined at low and high strains. While the two hypoxic groups were not significantly different from each other, both were significantly different from control ($P < 0.001$; Fig. 4). Damping coefficient, which measures the pressure pulse damping capacity or tissue viscoelasticity, was greater in the 15-day group than in the 0-day group ($P < 0.05$; Fig. 4 ), and no other differences were significant.

## 3.3 Mechanobiological correlations

To assess the presumptive correlative relationships between mechanical–functional and biological–structural indicators of remodeling, $E_{\text{low strain}}$ was plotted versus elastin thickness and $E_{\text{high strain}}$ was plotted versus collagen thickness (Fig. 5a, b). To assess the linearity of these relationships, the regression analysis coefficients of determination ($R^2$) were measured, and to assess the trends in these relationships, the Spearman's rank correlation coefficients ($r_s$) were measured.

Between $E_{\text{low strain}}$ and elastin thickness, there was a moderately linear relationship ($R^2 = 0.49$) with a significant trend towards higher modulus with greater elastin thickness ($r_s = 0.62$, $P < 0.001$). Between $E_{\text{high strain}}$ and collagen thickness, there was a stronger linearity ($R^2$ =0.67) with a significant trend towards higher modulus with greater collagen thickness ($r_s = 0.72$, $P < 0.001$).

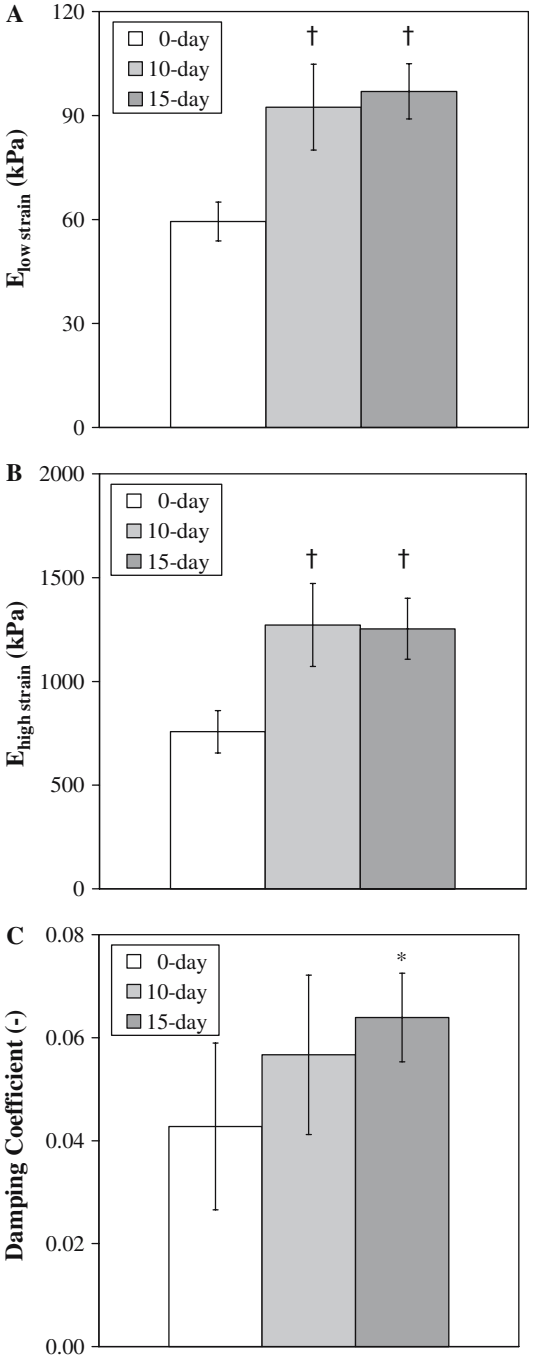


**Fig. 4** Dynamic mechanical properties for the 0-, 10- and 15-day groups. **a** Elastic modulus at low strain, **b** elastic modulus at high strain, and **c** damping coefficient. * $P < 0.05$ versus 0-day; † $P < 0.001$ versus 0-day

## 4 Discussion

Our results show that after 10 and 15 days of severe hypoxia, the main PAs of eNOS-null mice accumulate collagen and elastin, and have no change in SMC content. Mechanically, the PAs of eNOS-null mice exposed to hypoxia stretched

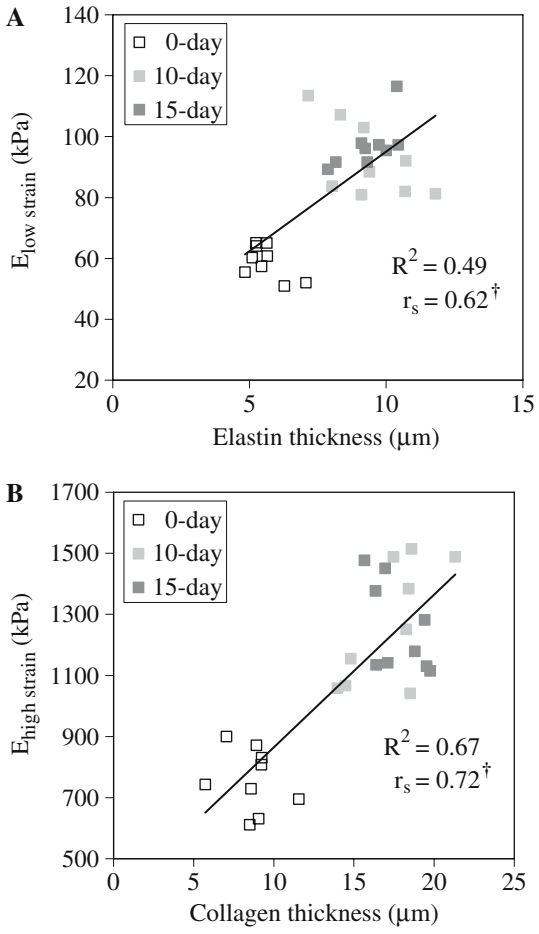


**Fig. 5** Correlations between **a** elastic modulus at low strain and elastin thickness and **b** elastic modulus at high strain and collagen thickness for all vessels. $R^2$ and $r_s$ values are provided in both panels. † $P < 0.001$

much less in response to pressure increases, had higher circumferential elastic moduli at all strains, and had higher damping coefficients than control vessels. The increase in low strain elastic modulus correlated with increased elastin thickness; the increase in high strain elastic modulus correlated with increased collagen thickness; and the increase in damping coefficient did not correlate significantly with any histologically measured wall components. These results are discussed in more detail in the following sections.

## 4.1 Histology and quantitative image analysis

As predicted, both collagen and elastin accumulated in response to severe hypertension in the eNOS-null mice. There was no appreciable change in SMC content despite an overall increase in wall thickness. Interestingly, while the amounts or thicknesses of collagen and elastin both increased with hypertension, only the percentage of collagen increased. The percent elastin in the wall remained relatively constant at 30%. Evidently, these structural changes occurred due to the increased solid wall stress created by the hypoxia-induced hypertension. Whereas increased muscularization of small arteries likely accounts for increases in pulmonary vascular resistance with severe hypertension in the eNOS-null mice, increased ECM components in the large arteries may change the pressure pulse transmission characteristics of the vasculature, leading to increased right ventricular workload.

## 4.2 Mechanical properties

### *4.2.1 Static behavior*

In all vessels, circumferential stretch increased with pressure for all pressures tested. Also, vessels exposed to hypertension stretched less at each pressure than those from normoxic controls. More interestingly, in vessels exposed to hypertension, the maximum circumferential stretch was reached at 40 mmHg whereas in normoxic controls circumferential stretch continued to significantly increase with pressure up to 60 mmHg. This finding is significant to vessel function since 40 mmHg is below the hypertensive systolic pressure of approximately 47 mmHg previously measured in eNOS-null mice exposed to two weeks of severe hypoxia (Fagan et al. 1999). A vessel that cannot stretch in response to a pulsatile pressure wave presents an increased resistance to flow (Zamir 2000). Therefore, these changes in circumferential stretch in eNOS-null mouse PAs in response to severe hypoxia may directly affect right ventricular energy requirements and contribute to right ventricular failure.

### *4.2.2 Dynamic behavior*

As measured dynamically, the circumferential elastic moduli of eNOS-null mouse PAs at both low and high strains increased with hypertension. These results correlate with the finding of increased pulmonary vascular stiffness in patients with primary pulmonary hypertension (Laskey et al. 1993). The characterization of elastic moduli at two different positions in the stress–strain curve was an effective method of determining the dynamic mechanical properties of this nonlinear material. It also allowed the correlation of these values with elastin and collagen content, which are primarily loaded under low strains and high strains, respectively. Incremental modulus also has been used to characterize vessel non-linear behavior by segmenting the stress-strain relationship into piece-wise linear relationships (Coulson et al. 2002).

The PA damping coefficient calculated from the dynamic stress-strain curve increased approximately 50% from 0-day vessels to 10- and 15-day hypoxic vessels. Cox also observed damping behavior in canine PAs; qualitatively, damping increased with increasing frequency (from 0.01 to 1 Hz) and decreased with smooth muscle cell activation (Cox 1984). Functionally, higher damping values in the hypoxic vessels indicate more energy dissipation through inelastic mechanisms during systolic pressure loading. Thus, with increased damping, the work required of the right heart increases, adding to the long-term stress on the heart and risk of ischemia.

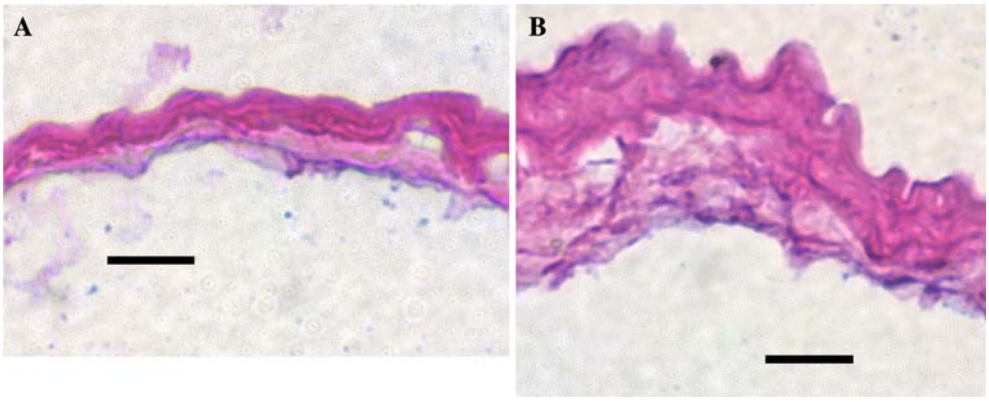


**Fig. 6** Representative images of proteoglycan staining of PAs from eNOS-null mice after **a** 0 and **b** 15 days of hypoxia. Alcian blue stains proteoglycans *blue*; other material stains *pink*. *Scale bar* is 20 $\mu$m

Both damping and stiffness changes may adversely affect the efficiency of ventricular-vascular coupling.

### 4.3 Mechanobiological correlations

One advantage of performing both mechanical–functional and biological–structural measurements on contralateral arteries during remodeling is the ability to correlate the mechanical changes with the biological changes. Our structure–function correlations (Fig. 5) support the hypotheses that increased elastic modulus at low strains occurs due to elastin accumulation and that increased elastic modulus at high strains occurs due to collagen accumulation. However, we must add two notes of caution. First, while the structure-function data from the 0-, 10- and 15-day conditions can be fit by linear regressions, we do not have direct evidence that data from intermediate time points would have intermediate values. That is, after 5 days of hypoxia, it is possible that collagen increases significantly but high strain elastic modulus does not. More data from different conditions are required to conclude that the high strain modulus–collagen thickness and low strain modulus–elastin thickness relationships are linear. Second, we would note that evidence of correlation (even with statistical significance) is not proof of causation. Since four of the six measured variables (low and high strain elastic moduli and collagen and elastin thicknesses) increased with hypoxia, correlations other than those for which we hypothesized causal relationships may have been significant. Experiments in which these mechanical properties are measured both before and after elastin or collagen degradation, such as have been performed in rabbit and dog arteries and veins (Dobrin and Canfield 1977; Kitoh et al. 1993), could address these issues.

Although SMC thickness increased as predicted, it did not correlate with the damping coefficient. Other important structural wall components and characteristics such as proteoglycans, ECM protein cross-linking, smooth muscle cell phenotype and vasoreactivity not measured in this study may be responsible for changes in damping coefficient. Proteoglycans in particular have been shown to contribute to the viscous damping coefficient in articular cartilage (Bader et al. 1992); however, their effects in vascular tissue are less clear. To assess the potential role of proteoglycans in vascular viscoelasticity, we performed a qualitative assay for proteoglycan content with an Alcian blue histological stain, which identifies mucopolysaccharides or glycosaminoglycans. Five specimens in each group (0-, 10- or 15-day) were observed. As shown by representative images (Fig. 6), proteoglycan content is present mostly in the adventitia and did not increase appreciably with hypoxia. Thus, proteoglycan content is unlikely to account for the increase in vascular viscoelasticity that occurs with hypoxia-induced pulmonary hypertension in the PAs of eNOS-null mice.

Based on the correlation between collagen thickness and high strain modulus, therapies that slow collagen synthesis or lead to collagen breakdown – either at the gene- or protein-level – may be effective at decreasing vascular stiffness at hypertensive pressures. In the aorta, some recently synthesized thiazolium compounds that selectively break protein cross-links and thereby reduce collagen stiffness, for example, have been found to decrease age-associated stiffening in monkeys (Vaitkevicius et al. 2001) and diabetes-associated stiffening in rats (Wolffenbuttel et al. 1998). These treatments were also successful in improving ventricular-vascular coupling, which may reduce the risk of heart failure.

### 4.4 Comparison to wild-type mice

The histological changes reported here in eNOS-null mice in response to hypoxia were comparable to those found in wild-type C57BL6 mice (Kobs et al. 2005), which are the genetic background for the eNOS-null strain. That is, in both mouse types, wall thickness, collagen thickness and elastin thickness increased with hypoxia-induced hypertension, and smooth muscle thickness was unchanged. An interesting difference is that in the congenital absence of eNOS, the average wall thickness was smaller at 0 days but not different after 10 or 15 days of hypoxia. Thus, the initial rate of change of wall thickness was faster in the absence of eNOS (from 0 to 10 days) and similar thereafter (from 10 to 15 days).

Analogous mechanical changes occurred in the two mouse types. In the wild-type strain, the tangent elastic modulus

increased with 10 and 15 days of exposure to hypoxia, and this increase correlated with the sum of elastin and collagen thickness (Kobs et al. 2005). Also, in the wild-type strain, the damping coefficient increased with hypoxia and did not correlate with smooth muscle cell content. The mechanical data are difficult to compare more precisely between mouse types since the previous and present studies were performed with different axial stretch ratios (1.12 vs. 1.4) and in different static and dynamic pressure ranges (5–25 mmHg vs. 5–60 mmHg). However, preliminary results in the wild-type strain with mechanical testing protocols identical to those used here suggest mechanical differences analogous to the biological ones: that in the congenital absence of eNOS, PAs stretch more at 0 days but are not different after 10 or 15 days of hypoxia (data not shown). Thus, the initial rate of change of static stiffness is faster in the absence of eNOS (from 0 to 10 days) and similar thereafter.

The somewhat confounding normalization of mechanobiological changes between 10 and 15 days may be explained by eNOS uncoupling. That is, under normal conditions, eNOS produces NO; however, under certain conditions, including hypertension (Takimoto et al. 2005) and possibly alveolar hypoxia (Archer et al. 1989, 1993; Chandel et al. 1998), eNOS uncoupling can occur such that eNOS produces more reactive oxygen species (ROS) than NO. In the absence of eNOS, this uncoupling reaction cannot occur, which may be protective of enhanced pathological vascular remodeling. Indeed, reducing ROS has been shown to normalize hypertension-induced remodeling in rat aortas (Pu et al. 2003) and in mice, the congenital absence of eNOS blunted systemic hypertension-induced left ventricular hypertrophy and dilation (Takimoto et al. 2005). In this case, the competing effects of increased vasoconstriction and decreased ROS production in the absence of eNOS may balance such that the chronic remodeling response is not different than in the presence of eNOS.

Future studies to quantify ROS generation in wild type and eNOS-null mouse lungs before and after chronic exposure to hypoxia are warranted. In addition, it is important to know whether the vascular mechanobiological states measured at 10 and 15 days are representative of those at even longer time points. Finally, these results do not answer the question of whether the eNOS-null mouse is an appropriate animal model of PPH. Our preliminary results suggest that it is not, but this suggestion must await a more quantitative comparison and possibly whole lung vascular mechanobiological studies.

### 4.5 Experimental considerations

In these experiments, we did not measure the residual stress in these arteries or use the zero-stress state as the reference state in the strain calculations. Takamizawa and Hayashi (1987) found that residual stress equalized the radial distribution of wall stress in canine carotid arteries. In rats exposed to 10 days of hypoxia, residual stress measurements on main PAs have shown that the outer wall grew more circumferentially than the inner wall, which also had the effect of equalizing the distribution of stress in the radial direction at the loaded state (Fung and Liu 1991). In these studies, the eNOS-null mouse PAs were thin enough that the radial distribution of stress could be ignored, but future studies to assess radial differences in growth rates in mouse PAs could yield further insight into the biomechanics of pulmonary vascular remodeling.

It was also assumed that mechanical end-effects were small. Since the average length-to-width ratio at 5 mmHg was 5.2:1 (the average suture-to-suture length was $2.7 \pm 0.4$ mm; the average maximum diameter was $0.52 \pm 0.04$ mm), it was reasonable to ignore end-effects at low pressures. However, this ratio decreased with increasing pressure as the diameter increased. At 60 mmHg, the average length-to-width ratio was 2.8:1, such that the vessels must be considered constrained by the end sutures. Given the short length and large diameter of the pulmonary artery in vivo, unconstrained test conditions for measuring tissue mechanical properties are not attainable even in principle. Nevertheless, there were no significant correlations or trends when axial length was compared with circumferential stretch within each group (data not shown). This finding suggests that shorter axial length had no significant effect on circumferential deformation or tissue mechanical properties measured in this study.

To perform the mechanical property calculations, we assumed the vessel walls were thin, incompressible, and homogeneous. The thin wall assumption was validated here for all 0-day vessels and 10- and 15-day vessels above 10 mmHg of pressure. The error incurred by using the thin wall stress formulation instead of the thick wall formulation (Timoshenko 1934) was less than 8% for all vessels at 5 mmHg transmural pressure ($5.6 \pm 0.9\%$) and less than 2% for all vessels at 60 mmHg ($1.7 \pm 0.4\%$). The incompressibility assumption of isolated mouse PAs has been shown to be valid elsewhere (Faury et al. 1999). Vasculature is inherently heterogeneous in the radial direction due to the layered nature of arteries and veins and often heterogeneous in the axial direction. However, the assumption of radial homogeneity is appropriate to a thin-wall analysis and insofar as we measured axial changes in biological properties, no differences were detected.

Finally, tissue injury or damage also may have affected our results. As shown by (von Maltzahn et al. 1984). in bovine carotid arteries, loss of adventitia will reduce the measured elastic modulus in isolated arteries. Extreme care was taken during excision to limit damage due to handling. More importantly, identical techniques were used to harvest right and left PAs; thus the absence of either intimal or adventitial damage that is evident histologically strongly suggests that the mechanically-tested vessels were similarly undamaged.

## 5 Conclusions

Hypoxia-induced pulmonary hypertension in the congenital absence of eNOS has been shown to induce significant pulmonary artery remodeling by collagen and elastin accumulation. Significant changes in large artery mechanical properties were also demonstrated, and these correlated

with measured histological changes. These results provide insight into the vascular structure, function, and structure–function relationships in large pulmonary arteries in this animal model. It remains unclear if the eNOS-null mouse is a better model of PPH than wild-type mice exposed to hypoxia. Elucidating the role of eNOS and endothelial-derived NO in large artery remodeling, pulmonary vascular function and right ventricular remodeling and dysfunction will yield insight into these complex processes.

**Acknowledgements** Funding support from National Institutes of Health COBRE grant P20RR15557, the UW-Madison College of Engineering, the Wisconsin Alumni Research Foundation and the Whitaker Foundation (Grant RG-02-0618) is gratefully acknowledged. We would also like to thank Nidal Muvarak for excellent histology work and Jens Eickhoff for guidance on the statistical analyses.

## References

Abman SH (1999) New developments in the pathogenesis and treatment of neonatal pulmonary hypertension. Pediatr Pulmonol Suppl 18:201–204

Archer SL, Nelson DP, Weir EK (1989) Simultaneous measurement of $O_2$ radicals and pulmonary vascular reactivity in rat lung. J Appl Physiol 67(5):1903–1911

Archer SL, Huang J, Henry T, Peterson D, Weir EK (1993) A redox-based $O_2$ sensor in rat pulmonary vasculature. Circ Res 73(6):1100–1112

Bader DL, Kempson GE, Egan J, Gilbey W, Barrett AJ (1992) The effects of selective matrix degradation on the short-term compressive properties of adult human articular cartilage. Biochim Biophys Acta 1116(2):147–154

Blitzer ML, Loh E, Roddy MA, Stamler JS, Creager MA (1996) Endothelium-derived nitric oxide regulates systemic and pulmonary vascular resistance during acute hypoxia in humans. J Am Coll Cardiol 28(3):591–596

Chandel NS, Maltepe E, Goldwasser E, Mathieu CE, Simon MC, Schumacker PT (1998) Mitochondrial reactive oxygen species trigger hypoxia-induced transcription. Proc Natl Acad Sci USA 95(20):11715–11720

Chesler NC, Thompson-Figueroa J, Millburne K (2004) Measurements of mouse pulmonary artery biomechanics. J Biomech Eng 126(2):309–314

Clark RH, Kueser TJ, Walker MW, Southgate WM, Huckaby JL, Perez JA, Roy BJ, Keszler M, Kinsella JP (2000) Low-dose nitric oxide therapy for persistent pulmonary hypertension of the newborn. N Engl J Med 342(7):469–474

Coulson RJ, Chesler NC, Vitullo L, Cipolla MJ (2002) Effects of ischemia and myogenic activity on active and passive mechanical properties of rat cerebral arteries. Am J Physiol Heart Circ Physiol 283(6):H2268–H2275

Cox RH (1984) Viscoelastic properties of canine pulmonary arteries. Am J Physiol 246(1 Pt 2):H90–H96

Dobrin P, Canfield T (1977) Identification of smooth muscle series elastic component in intact carotid artery. Am J Physiol 232(2):H122–H130

Fagan KA, Fouty BW, Tyler RC, Morris KG Jr, Hepler LK, Sato K, LeCras TD, Abman SH, Weinberger HD, Huang PL, McMurtry IF, Rodman DM (1999) The pulmonary circulation of homozygous or heterozygous eNOS-null mice is hyperresponsive to mild hypoxia. J Clin Invest 103(2):291–299

Faury G, Maher GM, Li DY, Keating MT, Mecham RP and Boyle WA (1999). Relation between outer and luminal diameter in cannulated arteries. Am J Physiol 277(5 Pt 2): H1745-H1753

Fung YC (1993) Biomechanics: mechanical properties of living tissues. 2nd ed. Springer, Berlin Heidelberg New York

Fung YC, Liu SQ (1991) Changes of zero-stress state of rat pulmonary arteries in hypoxic hypertension. J Appl Physiol 70(6):2455–2470

Giaid A, Saleh D (1995) Reduced expression of endothelial nitric oxide synthase in the lungs of patients with pulmonary hypertension. N Engl J Med 333(4):214–221

Kitoh T, Kawai Y, Ohhashi T (1993) Effects of collagenase, elastase, and hyaluronidase on mechanical properties of isolated dog jugular veins. Am J Physiol 265(1 Pt 2):H273–H280

Kobs RW, Muvarak NE, Eickhoff JC, Chesler NC (2005) Linked mechanical and biological aspects of remodeling in mouse pulmonary arteries with hypoxia-induced hypertension. Am J Physiol Heart Circ Physiol 288(3):H1209–H1217

Lakes R (1998) Viscoelastic solids. CRC Press, Boca Raton

Lane KB, Machado RD, Pauciulo MW, Thomson JR, Phillips JA III, Loyd JE, Nichols WC and Trembath RC (2000) Heterozygous germline mutations in BMPR2, encoding a TGF-beta receptor, cause familial primary pulmonary hypertension. The international PPH consortium. Nat Genet 26(1):81–84

Laskey WK, Ferrari VA, Palevsky HI, Kussmaul WG (1993). Pulmonary artery hemodynamics in primary pulmonary hypertension. J Am Coll Cardiol 21(2):406–412

Leeman M, de Beyl VZ, Delcroix M, Naeije R (1994) Effects of endogenous nitric oxide on pulmonary vascular tone in intact dogs. Am J Physiol 266(6 Pt 2):H2343–H2347

von Maltzahn WW, Warriyar RG, Keitzer WF (1984) Experimental measurements of elastic properties of media and adventitia of bovine carotid arteries. J Biomech 17(11):839–847

O'Rourke MF (1982) Vascular impedance in studies of arterial and cardiac function. Physiol Rev 62(2):570–623

Persson MG, Gustafsson LE, Wiklund NP, Moncada S, Hedqvist P (1990) Endogenous nitric oxide as a probable modulator of pulmonary circulation and hypoxic pressor response in vivo. Acta Physiol Scand 140(4):449–457

Pu Q, Neves MF, Virdis A, Touyz RM, Schiffrin EL (2003) Endothelin antagonism on aldosterone-induced oxidative stress and vascular remodeling. Hypertension 42(1):49–55

Rubin LJ (1997) Primary pulmonary hypertension. N Engl J Med 336(2):111–117

Steudel W, Ichinose F, Huang PL, Hurford WE, Jones RC, Bevan JA, Fishman MC, Zapol WM (1997) Pulmonary vasoconstriction and hypertension in mice with targeted disruption of the endothelial nitric oxide synthase (NOS 3) gene. Circ Res 81(1):34–41

Takamizawa K, Hayashi K (1987) Strain energy density function and uniform strain hypothesis for arterial mechanics. J Biomech 20(1):7–17

Takimoto E, Champion HC, Li M, Ren S, Rodriguez ER, Tavazzi B, Lazzarino G, Paolocci N, Gabrielson KL, Wang Y, Kass DA (2005) Oxidant stress from nitric oxide synthase-3 uncoupling stimulates cardiac pathologic remodeling from chronic pressure load. J Clin Invest 115(5):1221–1231

Thomson JR, Machado RD, Pauciulo MW, Morgan NV, Humbert M, Elliott GC, Ward K, Yacoub M, Mikhail G, Rogers P, Newman J, Wheeler L, Higenbottam T, Gibbs JS, Egan J, Crozier A, Peacock A, Allcock R, Corris P, Loyd JE, Trembath RC, Nichols WC (2000) Sporadic primary pulmonary hypertension is associated with germline mutations of the gene encoding BMPR-II, a receptor member of the TGF-beta family. J Med Genet 37(10):741–745

Timoshenko S (1934) Theory of elasticity. McGraw-Hill Book Company, New York

Vaitkevicius PV, Lane M, Spurgeon H, Ingram DK, Roth GS, Egan JJ, Vasan S, Wagle DR, Ulrich P, Brines M, Wuerth JP, Cerami A, Lakatta EG (2001) A cross-link breaker has sustained effects on arterial and ventricular properties in older rhesus monkeys. Proc Natl Acad Sci USA 98(3):1171–1175

Wolffenbuttel BH, Boulanger CM, Crijns FR, Huijberts MS, Poitevin P, Swennen GN, Vasan S, Egan JJ, Ulrich P, Cerami A, Levy BI (1998) Breakers of advanced glycation end products restore large artery properties in experimental diabetes. Proc Natl Acad Sci U S A 95(8):4630–4634

Zamir M (2000) The physics of pulsatile flow. AIP Press, New York